International Journal of Thermophysics, Vol. 23, No. 2, March 2002 (© 2002)

A Thermodynamic Property Model for Fluid-Phase Isobutane

H. Miyamoto[1, 2] and K. Watanabe[1]

Received May 1, 2001

A Helmholtz free energy equation of state for the fluid phase of isobutane (R-600a) has been developed on the basis of the ITS-90 temperature scale. This model was developed using selected measurements of the pressure–density–temperature (P, ρ, T), isobaric heat capacity, speed of sound, and saturation properties. The structure of the present model consists of only 19 terms in its functional form, which is the same as those successfully applied to our recent modeling of R-290 and R-600, and a nonlinear fitting procedure was used to determine the numerical parameters of the present equation of state. Based on a comparison with available experimental data, it is recognized that the model represents most of the reliable experimental data accurately in the range of validity covering temperatures from 113.56 K (the triple-point temperature) to 573 K, at pressures up to 35 MPa, and at densities up to 749 $kg \cdot m^{-3}$. Physically sound behavior of the derived thermodynamic properties over the entire fluid phase is demonstrated. The estimated uncertainties of properties calculated using the model are 0.2% in density, 1% in heat capacities, 0.02% in the speed of sound for the vapor, 1% in the speed of sound elsewhere, and 0.2% in vapor pressure, except in the critical region. In addition, graphical and statistical comparisons between experimental data and the available thermodynamic models, including the present one, showed that the model can provide a physically sound representation of all the thermodynamic properties of engineering importance.

KEY WORDS: equation of state; Helmholtz free energy; hydrocarbon; isobutane; natural working fluid; R-600a; refrigerant; thermodynamic properties.

1. INTRODUCTION

In accord with an increasing concern about the global warming impact, environmental-friendly refrigerants including hydrocarbons (HCs) are

[1] Department of System Design Engineering, Faculty of Science and Technology, Keio University, 3-14-1, Hiyoshi, Kohoku-ku, Yokohama 223-8522, Japan.
[2] To whom correspondence should be addressed. E-mail: miya@ws.sd.keio.ac.jp

0195-928X/02/0300-0477/0 © 2002 Plenum Publishing Corporation

currently expected to be the long-term alternatives that are benign to the global environment. HCs, including propane, *n*-butane, and isobutane, are also being considered as components of promising alternative mixtures with nonflammable hydrofluorocarbon (HFC) refrigerants since the flammability of HCs and larger global warming potential (GWP) values of HFCs can simultaneously be reduced by blending HCs with HFCs. It is noted, however, that there are far fewer available thermodynamic property data for isobutane (about 1600 data points) than for propane (about 3100 data points) and *n*-butane (about 2000 data points).

Taking this background into account, we have formulated an accurate Helmholtz free-energy type model for the fluid phase of isobutane (R-600a) by applying the same Helmholtz free-energy functional form as that applied in our models for propane (R-290) [1] and *n*-butane (R-600) [2]. We aimed to represent most of the experimental thermodynamic property data as accurately as the representation of the pressure-explicit MBWR model of Younglove and Ely [3], which has been widely used in various applications including REFPROP (Version 6.01) [4]. Note also that the present model has been developed not only to represent new experimental speed-of-sound data [5] that have recently become available since the Younglove and Ely model was developed, but also to adopt the new ITS-90 temperature scale.

2. SELECTION OF INPUT DATA

We compiled about 1600 experimental thermodynamic property measurements for isobutane. A summary of data in the single-phase region such as $P\rho T$, caloric, and acoustic property measurements, and saturation property data including vapor pressures, saturated-vapor and -liquid densities, and liquid heat capacities is listed in Table I. Most of the experimental thermodynamic property data reported prior to 1982 were summarized by Goodwin and Haynes [49]. For our modeling efforts, the temperature values of all experimental data are converted to ITS-90. It is noted, as also mentioned earlier, that the available experimental data for isobutane are much less than those of propane and *n*-butane. Recently, new experimental vapor-pressure data were reported by several groups [36–39] and these data are also included in Table I and carefully examined in Fig. 9, below. In the liquid phase, however, no new experimental caloric and acoustic property data have become available and only a qualitative test could be performed in this region in our modeling. It seems important, therefore, to carry out new reliable measurements of these derived properties, especially in the liquid phase.

Table I. Sources of Experimental Thermodynamic Property Data for Isobutane

				P		*ρ*		*T*	
First author[a]	Ref. no. (s.)	Property	No. of data	Range (MPa)	δP (kPa)	Range ($kg \cdot m^{-3}$)	$\delta\rho$ ($kg \cdot m^{-3}$)	Range (K)	δT (mK)
Sage	[6, 7]	$P\rho T$	567	0.1–34	1.4	1–594	0.1%	294–511	60
Morris	[8]	$P\rho T$	171	0.7–34	n.a.	10–593	n.a.	311–511	n.a.
Beattie*	[9]	$P\rho T$	75	2.6–31	n.a.	58–465	n.a.	423–573	n.a.
Gonzalez	[10]	$P\rho T$	5	55	n.a.	519–613	n.a.	311–444	n.a.
Waxman*	[11]	$P\rho T$	85	0.3–21	0.01%	6–458	n.a.	378–448	n.a.
Haynes*	[12]	$P\rho T$	156	1.7–35	n.a.	551–749	n.a.	120–300	n.a.
Sage	[6, 13]	C_P	59	0.1–2.4	0.1%			294–394	60
Dailey	[14]	C_P	8	0.1	n.a.			348–693	n.a.
Wacker*	[15]	C_P	37	0.0–0.1	n.a.			243–353	n.a.
Ernst*	[16]	C_P	21	0.0–0.8	n.a.			293–353	0.03%
Ewing*	[5]	W	79	0.0–0.1	0.2			251–320	3
Sage	[6]	P_S	7	0.3–2.9	1.4			294–394	60
Morris	[8]	P_S	2	1.1–2.2	n.a.			344–378	n.a.
Aston	[17]	P_S	9	0.0–0.1	n.a.			188–262	n.a.
Gilliland	[18]	P_S	5	1.4–3.7	n.a.			352–408	n.a.
Wackher	[19]	P_S	9	0.0–0.1	n.a.			206–263	n.a.
Beattie	[20]	P_S	5	0.4–3.1	n.a.			303–398	n.a.
Tickner	[21]	P_S	13	0.0–0.0	n.a.			122–187	300
Connolly	[22]	P_S	6	1.1–3.6	n.a.			344–407	n.a.
Hipkin	[23]	P_S	4	0.1–2.9	n.a.			267–394	n.a.
Hirata	[24]	P_S	29	0.3–2.0	n.a.			295–374	n.a.
Hirata	[25]	P_S	5	0.1–2.0	5			249–374	100
Besserer	[26]	P_S	4	0.5–3.0	21			311–394	n.a.
Kahre	[27]	P_S	5	0.2–0.8	n.a.			278–328	n.a.
Steele	[28]	P_S	10	0.2–1.1	0.05%			278–344	n.a.
Martinez–Ortiz	[29]	P_S	9	0.2–1.1	0.14			278–344	10
Waxman*	[30]	P_S	16	0.4–3.1	n.a.			298–398	n.a.
Weber	[31–33]	P_S	13	0.1–3.2	3			250–400	25
Leu	[34, 35]	P_S	8	1.1–3.1	0.15%			344–398	100
Higashi	[36]	P_S	5	0.2–0.5	5			283–313	10
Lim	[37]	P_S	8	0.4–0.9	1			302–333	100
Lim	[38]	P_S	4	0.2–0.9	5			283–333	50
Lee	[39]	P_S	4	0.3–0.7	1			293–323	10
Sage	[6]	ρ''	7			8–104	0.1%	294–394	60
Sliwinski*	[40]	ρ''	10			6–50	0.05	283–368	n.a.
Waxman*	[11]	ρ''	2			63–99	n.a.	378–394	n.a.
Sage	[6]	ρ'	7			379–559	0.1%	294–394	60
Morris	[8]	ρ'	3			422–537	n.a.	311–378	n.a.
Benoliel	[41]	ρ'	9			557–645	n.a.	213–293	n.a.
Wackher	[19]	ρ'	6			581–635	n.a.	224–273	n.a.
Beattie	[20]	ρ'	5			353–549	1	303–398	n.a.
Sliwinski*	[40]	ρ'	10			441–569	0.05	283–368	n.a.
Kahre	[27]	ρ'	5			510–576	n.a.	278–328	n.a.
Rodosevich	[42]	ρ'	3			736–741	0.1%	114–120	20
McClune*	[43]	ρ'	11			684–731	0.10%	123–173	100
Haynes*	[44]	ρ'	15			548–740	0.10%	115–300	40
Orrit*	[45]	ρ'	36			607–726	0.4	129–249	n.a.
Masui	[46]	ρ'	1			553	0.1%	297	10
Kaminishi	[47]	ρ'	6			518–580	0.2%	273–323	n.a.
Parks	[48]	C_σ	19					115–258	n.a.
Aston*	[17]	C_σ	25					117–257	n.a.

[a] Data used as input data are denoted with a superscript asterisk.

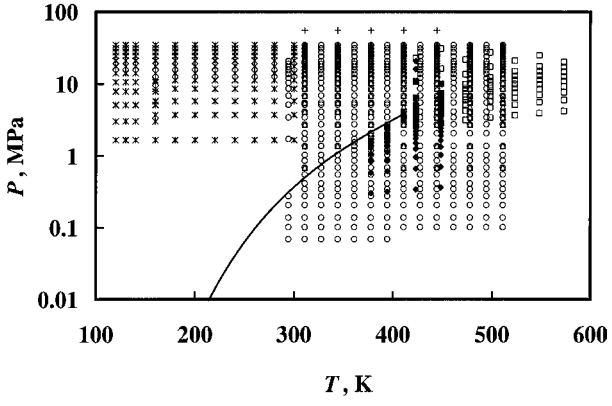

Fig. 1. Distribution of experimental $P\rho T$ property data. (○) Sage and Lacey [6, 7]; (△) Morris et al. [8]; (□) Beattie et al. [9]; (+) Gonzalez and Lee [10]; (♦) Waxman et al. [11]; (⁎) Haynes [12].

In the single-phase region, three sets of experimental $P\rho T$ property data, from Beattie et al. [9], Waxman et al. [11], and Haynes [12], which are indicated with superscript asterisks in Table I, were used as input data (Fig. 1). Other sets of $P\rho T$ data were used only to compare with the developed formulation; these include the data of Sage and Lacey [6, 7], Morris et al. [8], and Gonzalez and Lee [10]. Regarding caloric and acoustic properties (Fig. 2), three sets of experimental measurements in the

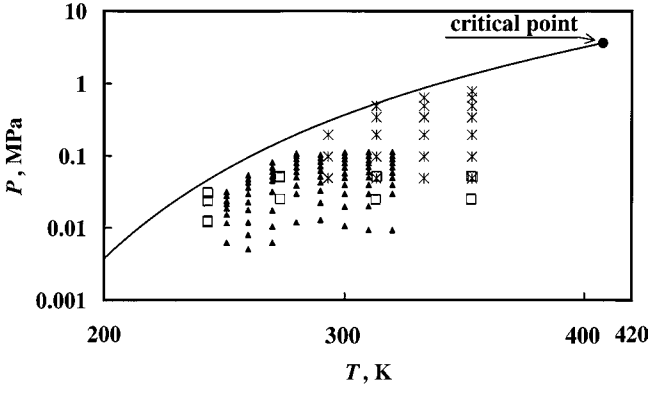

Fig. 2. Distribution of caloric and acoustic property data. (□) [C_P] Wacker et al. [15]; (⁎) [C_P] Ernst and Büsser [16]; (▲) [W] Ewing and Goodwin [5].

Table II. Summary of Available Critical Parameters for Isobutane[a, b]

First author	Ref. no.	Year	P_c (MPa)	ρ_c (kg·m^{-3})	T_c (K)
NGAA	[50]	1945	3.658	233.17	407.130
Beattie	[20]	1949	3.6477	220.86	408.111
Matteson	[51]	1950	3.648	220.93	408.108
Connolly	[22]	1962	3.6325	—	407.737
Hirata	[24]	1966	3.6477	—	408.131
Das	[52]	1973	3.6477	221	408.097
Goodwin	[49]	1982	3.640*	224.36*	407.817*
Levelt Sengers	[53]	1983	3.629	225.5	407.807
Stephan	[54]	1987	3.648	221.00	408.117

[a] All temperature values in this table were converted to ITS-90.
[b] Critical parameter values used for our modeling are denoted with a superscript asterisk.

vapor phase, i.e., two sets of isobaric heat capacity, C_P, data, from Wacker et al. [15] and Ernst and Büsser [16], and a new set of speed-of-sound, W, data, from Ewing and Goodwin [5], were also used as input data. The experimental isobaric heat capacity, C_P, data of Sage et al. [6, 13] were not used as input data.

The saturation property data used for our modeling are also indicated with superscript asterisks in Table I. Regarding the vapor pressures, P_S, and saturated-vapor and -liquid densities, ρ'' and ρ', these selected data were used to provide three sets of supplementary input data calculated from the ancillary correlations discussed in the next section. The saturated-liquid heat capacity, C_σ, data of Parks et al. [48] and Aston et al. [17] were directly used as additional input data only in the nonlinear fitting process.

A summary of reported critical parameter values is listed in Table II. For our modeling, the values of the critical temperature, density, and pressure determined by Goodwin and Haynes [49] are adopted. The experimental critical temperature and density values of Levelt Sengers et al. [53], which were determined by observation of the disappearance of the meniscus, agree with the values of Goodwin and Haynes within their reported uncertainties [53].

3. ANCILLARY CORRELATIONS

In the present study, the following three ancillary correlations for P_S, ρ'', and ρ' were developed on the basis of the selected experimental data indicated with superscript asterisks in Table I.

Table III. Coefficients of Eqs. (1)–(3)

i	A_i	B_i	C_i
1	−6.995565	−1.523942	1.60562
2	1.754758	−4.792479	−2.374095
3	−1.833831	−9.282003	2.098763
4	−2.19197	−26.37251	
5		−85.56735	

$$\ln \frac{P_S}{P_C} = \frac{1}{1-x}\left(A_1 x + A_2 x^{1.5} + A_3 x^{2.5} + A_4 x^{4.5}\right) \tag{1}$$

$$\ln \frac{\rho''}{\rho_C} = B_1 x^{0.33} + B_2 x^{0.8} + B_3 x^{2.3} + B_4 x^{4.4} + B_5 x^{10} \tag{2}$$

$$\ln \frac{\rho'}{\rho_C} = C_1 x^{0.33} + C_2 x + C_3 x^{1.1} \tag{3}$$

Equations (1)–(3) correspond to the vapor pressure, saturated-vapor density, and saturated-liquid density, respectively. In each correlation, $x = 1-T/T_C$, where T_C denotes the critical temperature, 407.817 K, P_C is the critical pressure, 3.640 MPa, and ρ_C is the critical density, 224.36 $kg \cdot m^{-3}$, as discussed in Section 2, and the coefficients are listed in Table III. In our development of these ancillary correlations, we used a set of P_S values which were determined using the simple calculation process of Zhang [55] based on the Clausius–Clapeyron equation and a set of ρ'' values calculated from Eq. (1) with a truncated virial equation of state with the same functional form that we used for propane [1]. It was developed based on the available $P\rho T$ property data in the vapor phase of isobutane below the critical temperature so as to generate additional ρ'' values at temperatures below the normal boiling point (261 K), where no measurements exist. It is noted that these two sets of calculated values, both of which are also included in Figs. 9 and 10 as filled squares, were also used to cover the range of temperatures below 261 K, and therefore, Eqs. (1)–(3) are valid for temperatures from the triple point (113.56 K) to the critical point (407.817 K).

4. FUNDAMENTAL EQUATION OF STATE

The dimensionless Helmholtz free-energy, $\phi(\tau, \delta)$, model is given by Eq. (4), where the ideal-gas state contribution, $\phi^0(\tau, \delta)$, is expressed by

Eq. (5), and the residual real-fluid contribution, $\phi^r(\tau, \delta)$, by Eq. (6). Independent variables are the inverse reduced temperature, $\tau = T_C/T$, and the reduced density, $\delta = \rho/\rho_C$, while f denotes the Helmholtz free energy.

$$\phi(\tau, \delta) = \frac{f}{RT} = \phi^0(\tau, \delta) + \phi^r(\tau, \delta) \tag{4}$$

$$\phi^0(\tau, \delta) = \ln \delta + a_1^0 + a_2^0 \tau + a_3^0 \ln \tau + \sum_{i=4}^{7} a_i^0 \ln[1 - \exp(-n_i \tau)] \tag{5}$$

$$\phi^r(\tau, \delta) = \sum_{i=1}^{8} a_i \tau^{t_i} \delta^{d_i} + \sum_{i=9}^{13} a_i \tau^{t_i} \delta^{d_i} \exp(-\delta) + \sum_{i=14}^{16} a_i \tau^{t_i} \delta^{d_i} \exp(-\delta^2) + \sum_{i=17}^{19} a_i \tau^{t_i} \delta^{d_i} \exp(-\delta^3) \tag{6}$$

In the present model, $T_C = 407.817$ K and $\rho_C = 224.36$ kg·m^{-3}, determined by Goodwin and Haynes [49], are used as reducing parameters. R is the gas constant for isobutane with $R = R_m/M$, where the universal gas constant, $R_m = 8.314472$ J·mol^{-1}·K^{-1} [56], and M is the molar mass, $M = 58.1222$ g·mol^{-1} [57].

The coefficients of $\phi^0(\tau, \delta)$ are listed in Table IV. In Eq. (5), the first term, ln δ, is related to the ideal-gas law, and the coefficients a_1^0 and a_2^0 are determined in accord with the reference values of specific enthalpy and specific entropy for the saturated liquid at $T_0 = 273.15$ K, which are $h'(T_0) = 200$ kJ·kg^{-1} and $s'(T_0) = 1.0$ kJ·kg^{-1}·K^{-1}. The ideal-gas heat capacity, C_P^0, values determined by Chen et al. [58] are reproduced within $\pm 0.03\%$ by Eq. (5) for temperatures from 50 to 1500 K.

The values of the coefficients of the residual real-fluid contribution, $\phi^r(\tau, \delta)$, are also listed in Table V. The structure and the combination of

Table IV. Coefficients of Eq. (5)

i	a_i^0	n_i
1	−6.026745	—
2	5.035251	—
3	3.059347	—
4	4.940314	0.9508183
5	4.090139	2.383449
6	9.739581	10.38655
7	15.68832	4.347095

Table V. Coefficients and Exponents of Eq. (6)

i	a_i	t_i	d_i
1	2.892737×10^{-1}	−0.25	1
2	-1.342570×10^{0}	1.5	1
3	-7.976713×10^{-3}	−0.75	2
4	2.025793×10^{-1}	0	2
5	-4.241612×10^{-2}	1.25	3
6	2.617971×10^{-3}	1.5	5
7	5.068955×10^{-5}	0.5	8
8	-1.144596×10^{-6}	2.5	8
9	-1.930153×10^{0}	1.5	3
10	1.982609×10^{0}	1.75	3
11	2.076533×10^{-3}	−0.25	8
12	-4.958752×10^{-3}	3	5
13	1.377372×10^{-3}	3	6
14	-1.582662×10^{-1}	4	1
15	-4.961892×10^{-2}	2	5
16	9.451030×10^{-4}	−1	7
17	-3.037276×10^{-2}	2	2
18	-1.382675×10^{-2}	19	3
19	8.876254×10^{-5}	5	15

terms of $\phi^{r}(\tau, \delta)$ were the same as those of the models for propane [1] and *n*-butane [2] developed by the present authors, and the nonlinear fitting process was used for adjusting the coefficients, a_i, to any thermodynamic property data simultaneously. The present model is developed on the basis of ITS-90, and the range of validity of Eq. (4) covers temperatures from 113.56 K (the triple-point temperature) to 573 K, at pressures up to 35 MPa, and at densities up to 749 $kg \cdot m^{-3}$.

5. COMPARISON WITH EXPERIMENTAL DATA

The ideal-gas part of the equation of state is based on the calculated ideal-gas heat capacity, C_P^0, determined from the spectroscopic data of Chen et al. [58], and the model represents all of the data from 50 to 1500 K within ±0.03%. The correlation for the ideal-gas heat capacity proposed by Jaeschke and Schley [59] also adopted the values of Chen et al. [58] as shown in Fig. 3. The C_P^0 data derived from the isobaric heat capacity measurements by Ernst and Büsser [16] are represented with a maximum relative deviation of ±0.13%, and the C_P^0 data derived from the speed-of-sound measurements by Ewing and Goodwin [5] are also represented within ±0.41%, with systematic deviations as shown in Fig. 3.

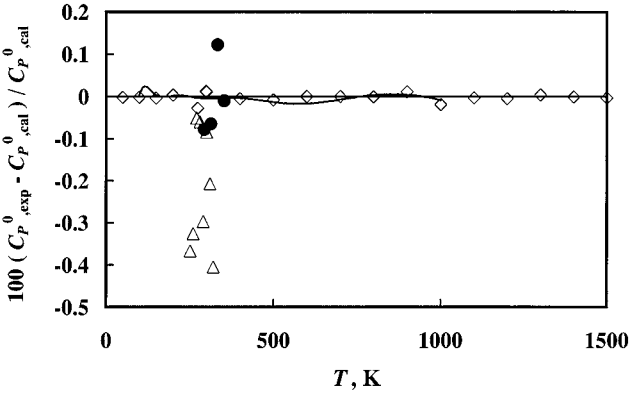

Fig. 3. Deviations of ideal-gas heat capacities C_P^0 from the present model. (◇) Chen et al. [58]; (●) Ernst and Büsser [16]; (△) Ewing and Goodwin [5]; (——) Jaeschke and Schley correlation [59].

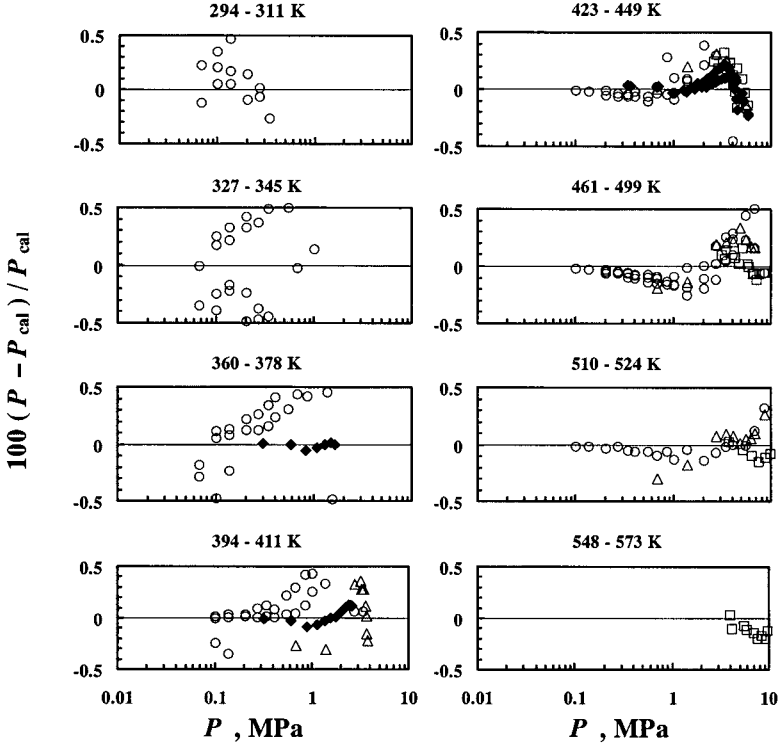

Fig. 4. Pressure deviations of $P\rho T$ property data from Eq. (4). (○) Sage and Lacey [6,7]; (△) Morris et al. [8]; (□) Beattie et al. [9]; (♦) Waxman et al. [11].

Pressure deviations of available $P\rho T$ property measurements in the vapor phase from the present model are shown in Fig. 4, while density deviations in the liquid phase are given in Fig. 5. For the vapor phase, the measurements by Waxman et al. [11] are well represented, within $\pm 0.23\%$, for pressure, whereas the data of Beattie et al. [9] agree with Eq. (4) within $\pm 0.32\%$ for pressure, as shown in Fig. 4. The $P\rho T$ data of Morris et al. [8], which were not used as input data, are represented within $\pm 0.36\%$, for pressure. The unused data of Sage and Lacey [6, 7] are represented within

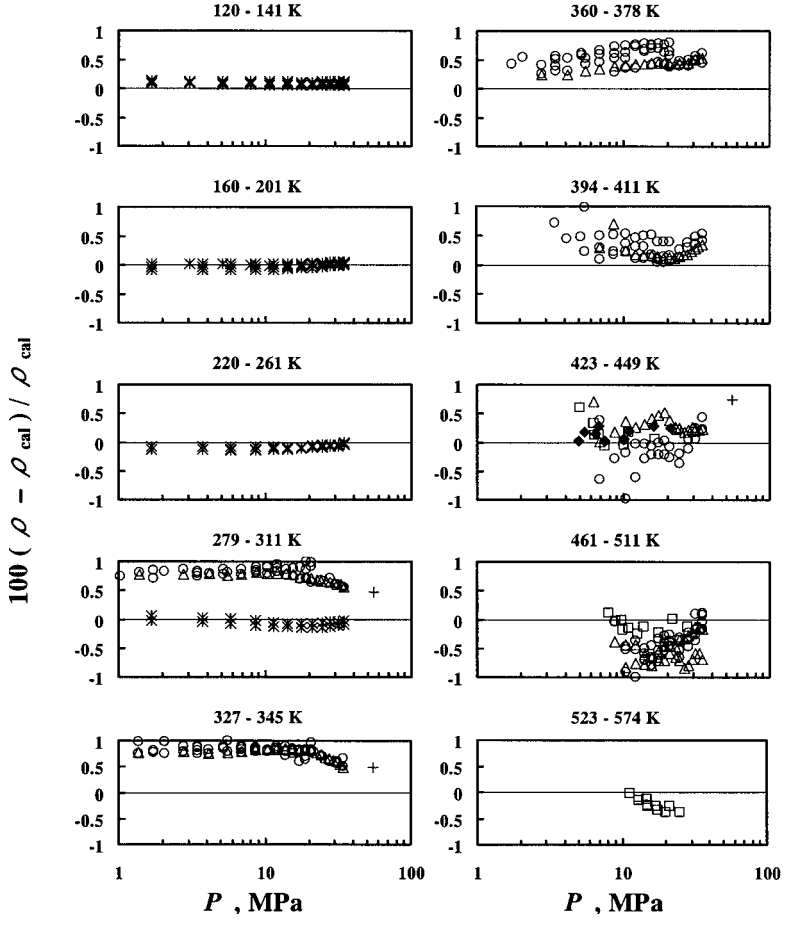

Fig. 5. Density deviations of $P\rho T$ property data from Eq. (4). (○) Sage and Lacey [6, 7]; (△) Morris et al. [8]; (□) Beattie et al. [9]; (+) Gonzalez and Lee [10]; (♦) Waxman et al. [11]; (⁎) Haynes [12].

$\pm 2.24\%$, for pressure, and are off-scale from Fig. 4, and the absolute average deviation (AAD) with respect to the data set of Sage and Lacey is less than 0.39%. In the liquid phase, the accurate $P\rho T$ data of Haynes [12] are represented within $\pm 0.15\%$ for density, while the data of Waxman et al. [11] and Beattie et al. [9] agree with Eq. (4) within ± 0.29 and $\pm 0.39\%$ for density except for three data points in each series, as shown in Fig. 5. The maximum deviations of unused $P\rho T$ data of Sage and Lacey [6,7] and Morris et al. [8] are off-scale from Fig. 5, and the AAD with respect to each data set is 0.65% and 0.63%, respectively.

Figures 6 through 8 show the relative deviations of the experimental C_P and W data from Eq. (4). It is clear from these three figures that most of the available measurements for the caloric and acoustic properties of isobutane are satisfactorily represented, within $\pm 0.5\%$, over the effective range of the present model. In the vapor phase, the C_P data of Wacker et al. [15] are well represented, within $\pm 0.13\%$, whereas the data of Ernst and Büsser [16] are represented within 0.44% except for a single datum near the saturation boundary, as shown in Fig. 6. The most recent and highly accurate W data of Ewing and Goodwin [5] in the vapor phase are well represented, within $\pm 0.023\%$, as shown in Fig. 7, in which the relative deviations between the values calculated from the Younglove and Ely model [3] and those from the present model are also included for detailed comparison. Along the saturation boundary, the C_σ data of Parks et al. [48] and Aston et al. [17] are reasonably well represented within $\pm 0.58\%$ at temperatures from 115 to 258 K, as shown in Fig. 8.

Comparisons of thermodynamic properties along the saturation boundary with the present model are shown in Figs. 9 through 11. The calculated values from the three ancillary correlations for P_S, ρ'', and ρ' given in Eqs. (1)–(3) are represented within $\pm 0.7\%$ in the range of validity of the present model except for the ρ'' and ρ' values close to the critical temperature, as clearly shown in Figs. 9 through 11. The present model represents the P_S measurements of Waxman and Gallagher [30] within $\pm 0.14\%$, while the present calculated P_S values based on the Clausius–Clapeyron equation at lower temperatures agree with the present equation of state within $\pm 0.21\%$ (± 0.2 kPa). As shown in Figs. 10 and 11, the ρ'' data of Sliwinski [40] and Waxman et al. [11] are represented within $\pm 0.50\%$, while the ρ' data of Sliwinski [40], McClune [43], Haynes and Hiza [44], and Orrit and Laupretre [45] are well represented, within $\pm 0.28\%$. Significant deviations of the ρ'' data of Sage and Lacey [6] and the ρ' data of Sage and Lacey [6], Morris et al. [8], and Beattie et al. [20] are also shown in Figs. 10 and 11.

As one of the most important tests for the accuracy of a thermodynamic property model, the behaviors of the isochoric heat capacity, C_V,

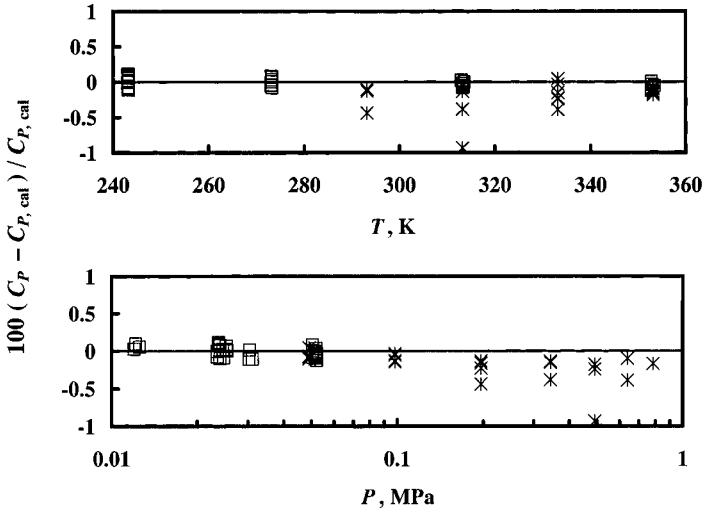

Fig. 6. Deviations of the isobaric heat capacity data in the vapor phase from Eq. (4). (□) Wacker et al. [15]; (⁎) Ernst and Büsser [16].

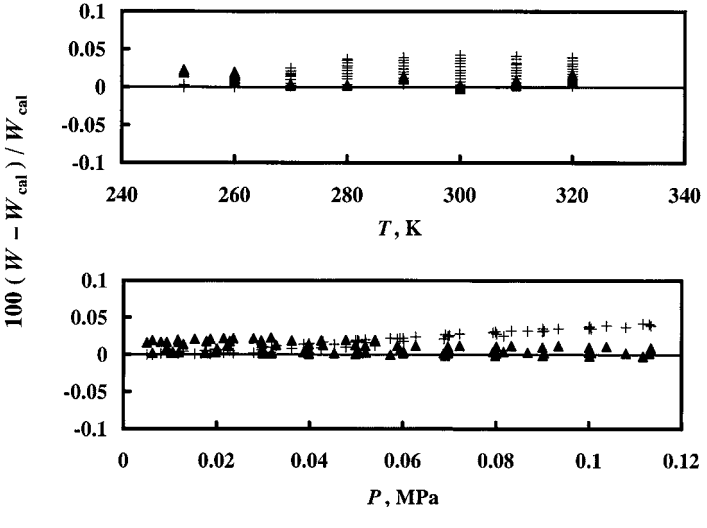

Fig. 7. Deviations of the speed-of-sound data in the vapor phase from Eq. (4). (▲) Ewing and Goodwin [5]; (+) calculated values from Younglove and Ely model [3].

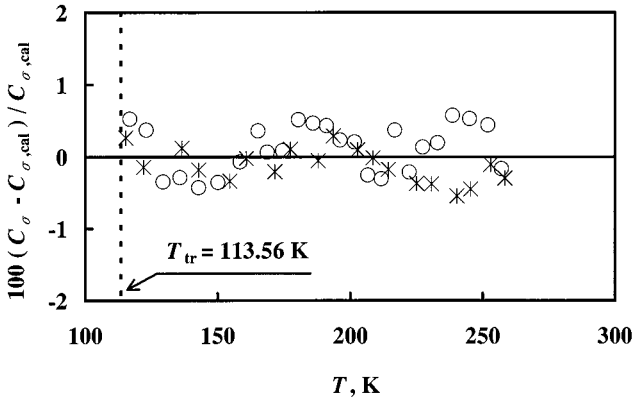

Fig. 8. Deviations of the saturated-liquid heat capacity data from Eq. (4). (⁎) Parks et al. [48]; (○) Aston et al. [17].

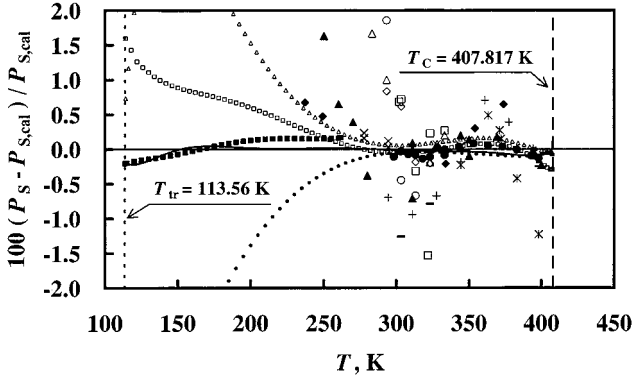

Fig. 9. Deviations of measured and calculated vapor pressure values from the present model. (+) Sage and Lacey [6]; (—) Beattie et al. [20]; (♦) Hirata et al. [25], (×) Martinez-Ortiz and Manley [29]; (●) Waxman and Gallagher [30]; (▲) Weber [31–33]; (⁎) Leu and Robinson [34, 35]; (○) Higashi et al. (additional two data points: +3.7%, +4.6%) [36]; (□) Lim et al. (additional single datum point: −3.0%) [37]; (△) Lim et al. [38]; (◇) Lee et al. [39]; (■) calculated values based on the Clausius–Clapeyron equation; (——) Eq. (1); (· · ·) Younglove and Ely model [3]; (△△△) Span model [60]; (□□□) Zhang and Watanabe model [61].

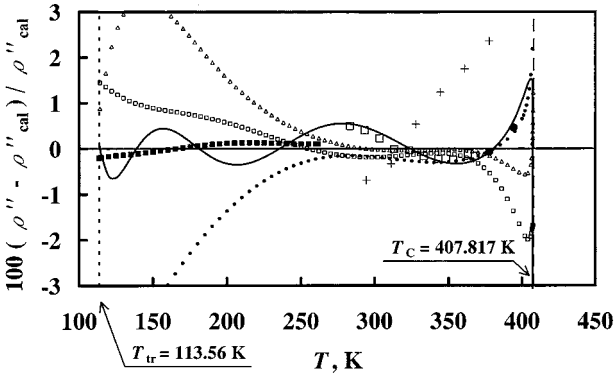

Fig. 10. Deviations of measured and calculated saturated-vapor densities ρ'' from the present model. (+) Sage and Lacey [6]; (□) Sliwinski [40]; (●) Waxman et al. [11]; (■) calculated values from the ancillary virial equation of state; (——) Eq. (2); (· · ·) Younglove and Ely model [3]; (△△△) Span model [60]; (□□□) Zhang and Watanabe model [61].

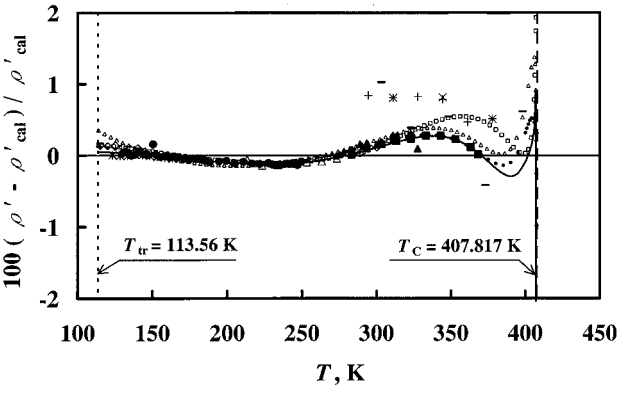

Fig. 11. Deviations of measured and calculated saturated-liquid densities ρ' from the present model. (+) Sage and Lacey [6]; (×) Morris et al. [8]; (△) Benoliel [41]; (—) Beattie et al. [20]; (■) Sliwinski [40]; (▲) Kahre [27]; (⁎) McClune [43]; (◇) Haynes and Hiza [44]; (●) Orrit and Laupretre [45]; (♦) Kaminishi et al. [47]; (——) Eq. (3); (· · ·) Younglove and Ely model [3]; (△△△) Span model [60]; (□□□) Zhang and Watanabe model [61].

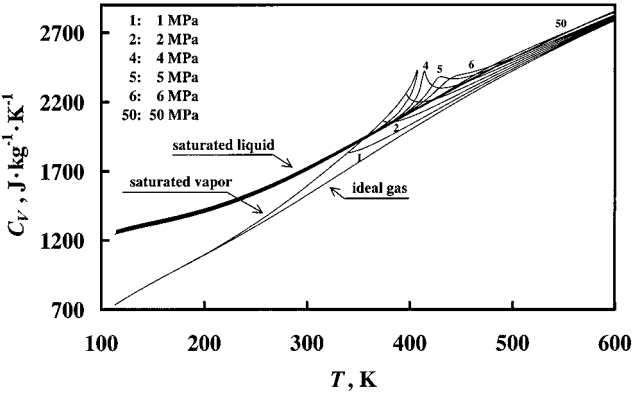

Fig. 12. Calculated isochoric heat capacity values along isobars using the present model.

isobaric heat capacity, C_P, speed of sound, W, and Joule–Thomson coefficients, μ, over an extended range of temperature and pressure are shown in Figs. 12 through 15, respectively. From the physically reasonable behaviors demonstrated in these four figures over the entire range including the extrapolated region where no experimental data are available, it is confirmed that the present model exhibits a satisfactory thermodynamic consistency over the entire fluid phase of isobutane.

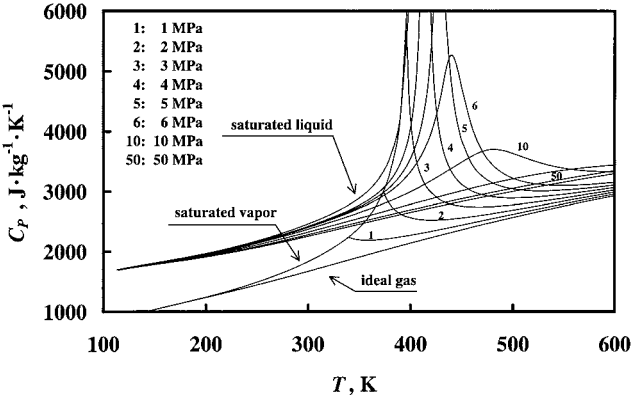

Fig. 13. Calculated isobaric heat capacity values along isobars using the present model.

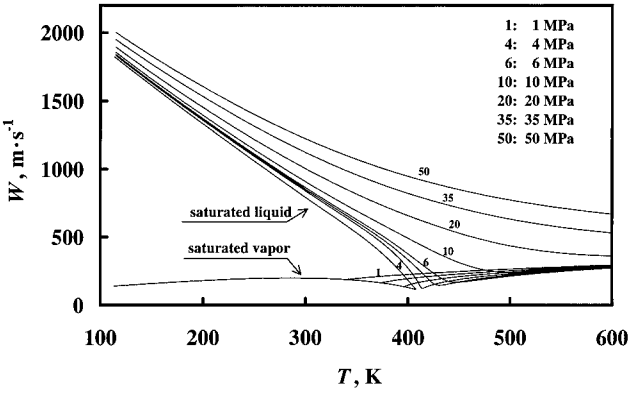

Fig. 14. Calculated speed-of-sound values along isobars using the present model.

6. COMPARISON WITH EXISTING MODELS

We compare the present model with three other representative models, i.e., those of Younglove and Ely [3], Span [60], and Zhang and Watanabe [61], to confirm its reliability with the aid of graphical and statistical examinations.

The model developed by Younglove and Ely [3] is a modified BWR equation of state with 32 coefficients. Its range of validity covers temperatures up to 600 K and pressures up to 35 MPa. Its high reproducibility regarding the available thermodynamic property measurements are confirmed

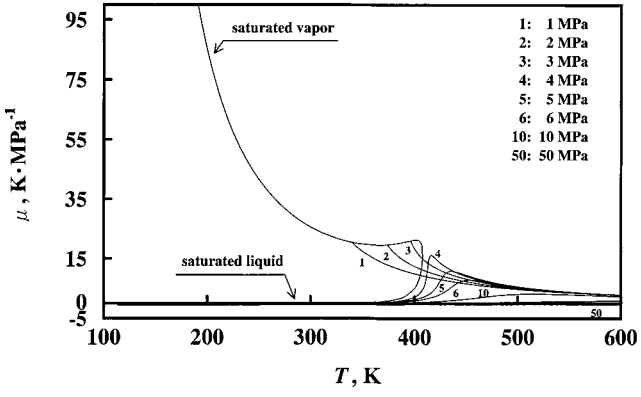

Fig. 15. Calculated Joule–Thomson coefficient values along isobars using the present model.

in the fluid phase of isobutane, especially in the liquid phase and at the saturation boundary, and this model is currently adopted in the software package, REFPROP (Version 6.01), published by NIST [4]. We used subroutines given in the source program of REFPROP (Version 6.01) for comparing the Younglove and Ely model with experimental data. For precise comparison, the temperature scale of the Younglove and Ely model was converted from IPTS-68 to ITS-90.

The other models with which we compared are the Helmholtz free-energy equations of state developed by Span [60] and Zhang and Watanabe [61]. The Span model has an excellent reproducibility in the vapor phase, and the total number of terms for the residual part is only 12. It is also important to note that Span is applying the same combination of terms with his model to 15 nonpolar substances. The Zhang and Watanabe model has 24 terms in the residual part, and the functional form of this equation of state has been determined only for isobutane. The coefficients and exponents of this equation of state are not published.

Comparisons of essential thermodynamic properties along the saturation boundary with the present model are shown in Figs. 9 through 11. It is verified in these three figures that the representation regarding the saturation boundary of the four models are similar except at lower temperatures, below the normal boiling point (261 K). As discussed earlier, in this temperature range, we developed ancillary correlations for P_S and ρ'', which fall between the existing models. The numerical differences of P_S and ρ'' values at the triple point (113.56 K) are less than 2 mPa and 1×10^{-7} $\mathrm{kg \cdot m^{-3}}$, respectively, between our model and the other three models. At low pressures and temperatures, however, the calculated heat capacity value is very sensitive to the first and second temperature differentials of the P_S curve and the first temperature differential of the ρ'' curve. C_V and C_P values at such low temperatures and pressures calculated from the four models mentioned above are examined in Figs. 16 and 17, respectively. In Fig. 16, the calculated C_V values from the present model and the Zhang and Watanabe model [61] show physically sound behaviors at low temperatures, below the triple point. The isobars of the Span model [60] also show smooth behavior at low temperatures and have minimum points at temperatures considerably higher than the triple point. It should be noted that this behavior of the Span model could also be observed with some other fluids, for example, R-32 [62]. On the other hand, the isobars of the Younglove and Ely model [3] cross. It is shown by Fig. 16, therefore, that we face a difficult situation for modeling at lower temperatures since no experimental C_V data are available in the liquid phase. On the other hand, no intersecting isobars for C_P values from the four models are shown in Fig. 17. It is shown in Fig. 17, however, that the saturated-liquid heat

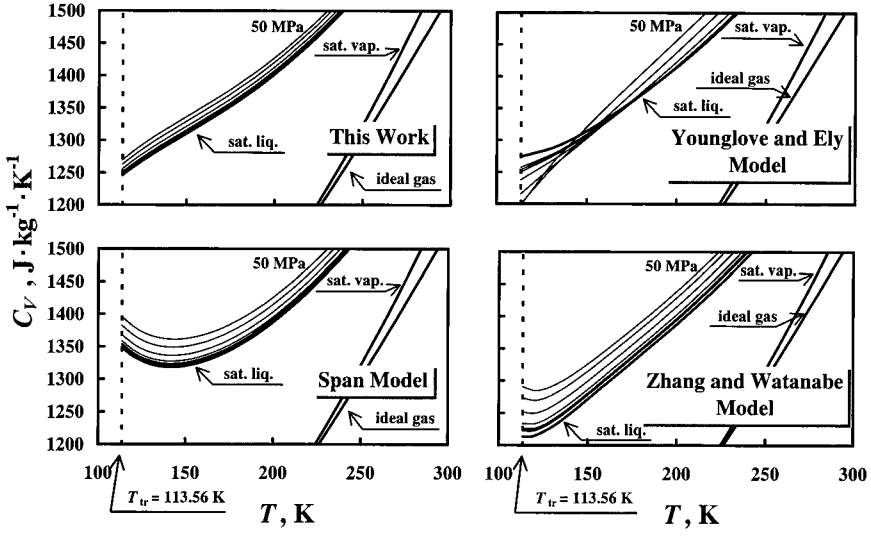

Fig. 16. Calculated isochoric heat capacity values along isobars using the present model, Younglove and Ely model [3], Span model [60], and Zhang and Watanabe model [61].

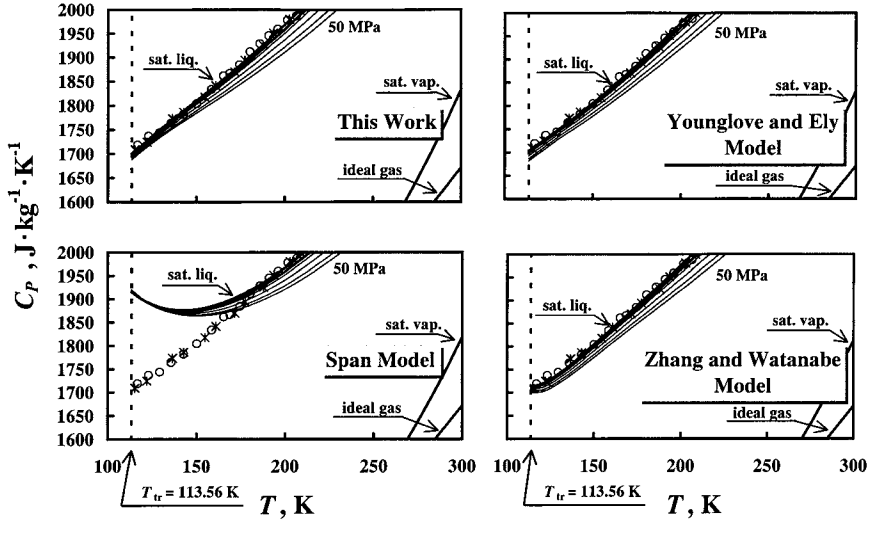

Fig. 17. Calculated isobaric heat capacity values along isobars using the present model, Younglove and Ely model [3], Span model [60], and Zhang and Watanabe model [61] and comparison with the measured saturated-liquid heat capacity data. (∗) Parks et al. [48]; (○) Aston et al. [17].

capacity, C_σ, data of Parks et al. [48] and Aston et al. [17] are well represented by the present model, the Younglove and Ely model [3], and the Zhang and Watanabe model [61], whereas C_P values calculated from the Span model [60] have significant deviations from experimental C_σ data. At low pressures and temperatures, it is known that C'_P and C_σ have nearly the same values and the following relation was discussed by Weber [63]:

$$C_\sigma \approx C'_P = C''_V - \frac{RT}{\rho''}\left(\frac{\mathrm{d}\rho''}{\mathrm{d}T}\right) + \frac{T}{\rho''^2}\left(\frac{\mathrm{d}\rho''}{\mathrm{d}T}\right)\left(\frac{\mathrm{d}P_S}{\mathrm{d}T}\right) - \frac{T}{\rho''}\left(\frac{\mathrm{d}^2P_S}{\mathrm{d}T^2}\right) \qquad (7)$$

where C''_V denotes the isochoric saturated-vapor heat capacity and R is the gas constant. Equation (7) clearly illustrates that there is a thermodynamic relationship between C_σ data and temperature differentials of P_S and ρ'' values. In general, especially in our model, the input ρ'' data were developed using the P_S values, and therefore, the developed model should represent the experimental C_σ data and the P_S and ρ'' values simultaneously at the same temperatures. In such circumstances, the present model meets the above-mentioned requirement and it could be concluded that the present model shows thermodynamic consistency even in this temperature and pressure region.

The accuracy and reliability of each model in the single-phase region were statistically examined in terms of the absolute average deviation (AAD), the bias (BIAS), the standard deviation (SDV), the root-mean-square deviation (RMS), and the maximum percentage deviation (MAX%) with respect to each data set as summarized in Table VI.

The statistical values in Table VI show that the present model satisfactorily reproduces the $P\rho T$ property data. In the vapor-phase region, the statistical results including AAD, BIAS, SDV, and RMS from the Younglove and Ely model [3] are slightly larger than those from the present model. Table VI also shows that the representation for the vapor phase of the Span model [60] and the Zhang and Watanabe model [61] are excellent. The numerical differences among the statistical values, however, are less than $\pm 0.1\%$ among our model and the three other models. As for the liquid-phase $P\rho T$ data, the above-mentioned statistical values calculated by the present model are slightly larger than those by the other three models, although the differences among the four models are negligibly small except for three experimental data of Waxman et al. [11] reported in the near-vicinity of the critical point.

Statistical comparisons of caloric and acoustic property data with all the models are also summarized in Table VI. In the vapor-phase region, the different representations of the four models regarding the speed-of-sound data of Ewing and Goodwin [5] are extremely small even though the

Table VI. Statistical Comparison of Four Models with Single-Phase Experimental Data[a]

Property	Phase	No. of data	First author	AAD	BIAS	SDV	RMS	MAX%	AAD	BIAS	SDV	RMS	MAX%
				Present model					Younglove and Ely model [3] (REFPROP Version 6.01 [4])				
$P\rho T$	V	274	Sage [6, 7]	0.39	−0.10	0.57	0.58	2.24	0.40	−0.12	0.60	0.61	2.38
$P\rho T$	V	36	Morris [8]	0.18	0.07	0.20	0.21	0.36	0.21	0.12	0.23	0.26	0.43
$P\rho T$	V	42	Beattie* [9]	0.11	−0.01	0.13	0.13	0.32	0.20	0.07	0.22	0.23	0.52
$P\rho T$	V	72	Waxman* [11]	0.08	0.05	0.09	0.10	−0.23	0.10	0.04	0.11	0.12	0.21
$P\rho T$	L	293	Sage [6, 7]	0.65	0.35	0.91	0.97	−11.89	0.55	0.24	0.90	0.93	−12.05
$P\rho T$	L	135	Morris [8]	0.63	0.38	0.86	0.94	6.33	0.58	0.33	0.86	0.92	6.04
$P\rho T$	L	33	Beattie* [9]	0.24	0.02	0.37	0.36	1.28	0.38	−0.27	0.38	0.46	−0.81
$P\rho T$	L	13	Waxman* [11]	0.43	0.43	0.54	0.68	1.48	0.21	0.04	0.28	0.27	−0.57
$P\rho T$	L	156	Haynes* [12]	0.07	−0.01	0.08	0.08	−0.14	0.02	−0.01	0.03	0.03	−0.08
C_P	V	59	Sage [6, 13]	7.42	−7.42	2.69	7.89	−17.90	7.70	−7.70	2.69	8.15	−18.17
C_P	V	37	Wacker* [15]	0.06	−0.02	0.07	0.07	−0.12	0.16	−0.16	0.09	0.18	−0.33
C_P	V	21	Ernst* [16]	0.21	−0.20	0.21	0.28	−0.93	0.50	−0.50	0.30	0.58	−1.06
W	V	79	Ewing* [5]	0.01	0.01	0.01	0.01	0.02	0.02	−0.01	0.02	0.02	−0.05
				Span model [60]					Zhang and Watanabe model [61]				
$P\rho T$	V	274	Sage [6,7]	0.39	−0.12	0.57	0.59	2.06	0.40	−0.13	0.57	0.58	1.92
$P\rho T$	V	36	Morris [8]	0.17	0.06	0.19	0.20	0.54	0.17	0.07	0.19	0.20	0.36
$P\rho T$	V	42	Beattie* [9]	0.11	0.11	0.13	0.17	0.57	0.08	0.07	0.05	0.09	0.15
$P\rho T$	V	72	Waxman* [11]	0.04	−0.02	0.05	0.05	−0.13	0.05	−0.03	0.05	0.06	−0.19
$P\rho T$	L	293	Sage [6,7]	0.51	0.15	0.90	0.91	−12.31	0.56	0.18	0.91	0.93	−12.11
$P\rho T$	L	135	Morris [8]	0.51	0.18	0.74	0.76	4.56	0.53	0.19	0.70	0.72	3.16
$P\rho T$	L	33	Beattie* [9]	0.41	−0.40	0.30	0.50	−0.78	0.12	−0.09	0.14	0.16	−0.44
$P\rho T$	L	13	Waxman*[11]	0.17	−0.11	0.28	0.29	−0.76	0.12	0.04	0.21	0.20	−0.50
$P\rho T$	L	156	Haynes* [12]	0.07	0.01	0.09	0.09	0.18	0.02	0.00	0.02	0.02	0.07
C_P	V	59	Sage [6, 13]	7.30	−7.30	2.65	7.76	−17.21	7.10	−7.09	2.69	7.58	−17.01
C_P	V	37	Wacker* [15]	0.06	−0.03	0.06	0.07	−0.13	0.16	0.15	0.12	0.19	0.35
C_P	V	21	Ernst* [16]	0.15	−0.14	0.08	0.16	−0.32	0.10	0.09	0.08	0.12	0.24
W	V	79	Ewing* [5]	0.01	0.01	0.01	0.01	0.02	0.01	0.00	0.01	0.01	−0.03

[a] Note that deviations of $P\rho T$ data are given with respect to densities in the liquid phase, whereas with respect to pressures in the vapor phase.

Younglove and Ely model [3] was developed without these data. The isobaric heat-capacity data of Wacker et al. [15] are better represented by the present model and the Span model [60] than by the Younglove and Ely model [3] and the Zhang and Watanabe model [61]. The Span model [60] shows a slightly better representation for the isobaric heat-capacity data of Ernst and Büsser [16]. More precisely, the difference in the reproducibility between the Span model and the present model exists only for a single datum near the saturation boundary. We believe, therefore, that the present model exhibits an almost-equivalent representation in the vapor phase, similar to the Span model. From the above-mentioned comparisons, it is reasonable to conclude that the present model also does a good job representing the reliable sets of caloric and acoustic property data in the vapor phase.

7. CONCLUSION

We have developed an equation of state for isobutane that is valid for temperatures from 113.56 K (the triple-point temperature) to 573 K, at pressures up to 35 MPa, and at densities up to 749 $kg \cdot m^{-3}$. For our model, the selected experimental data for $P\rho T$, caloric, acoustic, and saturation properties, and the present calculated P_S and ρ'' values at temperatures below the normal boiling point (261 K), where no measurements exist, were used as input data. As a result, the accurate experimental thermodynamic property data for isobutane are satisfactorily represented, and the smooth behavior of the calculated isochoric and isobaric heat capacities, speeds of sound, and Joule–Thomson coefficients has also been confirmed in the range of validity of the present model. The overall uncertainties of the equation of state are estimated to be about 0.2% for density, 1% for heat capacities, 0.02% for the speed of sound for the vapor, 1% for the speed of sound elsewhere, and 0.2% in vapor pressure, except in the critical region.

In addition, we have also discussed the reliability of three other models, proposed by Younglove and Ely, Span, and Zhang and Watanabe, in comparison with the present model. A statistical analysis has been extensively conducted among these four models. The present model showed an excellent thermodynamic consistency in representing the thermodynamic properties over the entire fluid phase of isobutane with a relatively short dimensionless Helmholtz free-energy function.

We note, again, that there are far fewer available thermodynamic property data for isobutane (about 1600 data points) than for propane and *n*-butane. Even in such a difficult circumstance for modeling, however, we could still examine the representation of vapor pressures using several sets of experimental data, which were reported in 1994, 1999, and 2000. These

data were useful in our model development, and additional measurements are encouraged.

ACKNOWLEDGMENTS

The authors are grateful to Dr. H.-L. Zhang, Sharp Corp., Japan, who kindly provided his calculation process package for the vapor pressures, which was useful in the present study. We also wish to express gratitude to Dr. E. W. Lemmon, NIST, who kindly provided a valuable set of information about available experimental data.

REFERENCES

1. H. Miyamoto and K. Watanabe, *Int. J. Thermophys.* **21**:1045 (2000).
2. H. Miyamoto and K. Watanabe, *Int. J. Thermophys.* **22**:459 (2001).
3. B. A. Younglove and J. F. Ely, *J. Phys. Chem. Ref. Data* **16**:577 (1987).
4. M. O. McLinden, S. A. Klein, E. W. Lemmon, and A. P. Peskin, *NIST Thermodynamic and Transport Properties of Refrigerants and Refrigerant Mixtures (REFPROP)*, Version 6.01 (U.S. Deptartment of Commerce, Washington, DC, 1998).
5. M. B. Ewing and A. R. H. Goodwin, *J. Chem. Thermodyn.* **23**:1107 (1991).
6. B. H. Sage and W. N. Lacey, *Ind. Eng. Chem.* **30**:673 (1938).
7. B. H. Sage and W. N. Lacey, *Monograph on API Research Project 37, American Petroleum Institute* (1950), pp. 58–69.
8. W. M. Morris, B. H. Sage, and W. N. Lacey, *Tech. Publ. No. 1128, Petroleum Technology* (1939).
9. J. A. Beattie, S. Marple, Jr., and D. G. Edwards, *J. Chem. Phys.* **18**:127 (1950).
10. M. H. Gonzalez and A. L. Lee, *J. Chem. Eng. Data* **11**:357 (1966).
11. M. Waxman, H. A. Davis, J. M. H. Levelt Sengers, and M. Klein, *Natl. Bur. Stand. (U.S.), Interagency Report NBSIR 79-1715* (1978).
12. W. M. Haynes, *J. Chem. Eng. Data* **28**:367 (1983).
13. B. H. Sage, D. C. Webster, and W. N. Lacey, *Ind. Eng. Chem.* **29**:1309 (1937).
14. B. P. Dailey and W A. Felsing, *J. Am. Chem. Soc.* **65**:44 (1943).
15. P. F. Wacker, R. K. Cheney, and R. B. Scott, *J. Res. Natl. Bur. Stand.* **38**:651 (1947).
16. G. Ernst and J. Büsser, *J. Chem. Thermodyn.* **2**:787 (1970).
17. J. G. Aston, R. M. Kennedy, and S. C. Schumann, *J. Am. Chem. Soc.* **62**:2059 (1940).
18. E. R. Gilliland and H. W. Scheeline, *Ind. Eng. Chem.* **32**:48 (1940).
19. R. C. Wackher, C. B. Linn, and A. V. Grosse, *Ind. Eng. Chem.* **37**:464 (1945).
20. J. A. Beattie, D. G. Edwards, and S. Marple, Jr., *J. Chem. Phys.* **17**:576 (1949).
21. A. W. Tickner and F. P. Lossing, *J. Phys. Colloid Chem.* **55**:733 (1951).
22. J. F. Connolly, *J. Phys. Chem.* **66**:1082 (1962).
23. H. Hipkin, *AIChE J.* **12**:484 (1966).
24. M. Hirata and S. Suda, *J. Jpn. Petrol. Inst.* **9**:885 (1966) [in Japanese].
25. M. Hirata, S. Suda, T. Hakuta, and K. Nagahama, *Mem. Fac. Technol. Tokyo Metrop. Univ.* **19**:103 (1969).
26. G. J. Besserer and D. B. Robinson, *J. Chem. Eng. Data* **18**:298 (1973).
27. L. C. Kahre, *J. Chem. Eng. Data* **18**:267 (1973).
28. K. Steele, B. E. Poling, and D. B. Manley, *J. Chem. Eng. Data* **21**:399 (1976).

29. J. A. Martinez-Ortiz and D. B. Manley, *J. Chem. Eng. Data* **23**:165 (1978).
30. M. Waxman and J. S. Gallagher,*J. Chem. Eng. Data* **28**:224 (1983).
31. L. A. Weber, *Cryogenics* **25**:338 (1985).
32. L. A. Weber, *J. Chem. Eng. Data* **34**:171 (1989).
33. L. A. Weber, *J. Chem. Eng. Data* **34**:452 (1989).
34. A.-D. Leu and D. B. Robinson, *J. Chem. Eng. Data* **32**:444 (1987).
35. A.-D. Leu and D. B. Robinson, *J. Chem. Eng. Data* **34**:315 (1989).
36. Y. Higashi, M. Funakura, and Y. Yoshida, *CFCs: The Day After, Proceedings of the Joint Meeting of IIR Commissions B1, B2, E1, and E2*, Padova, Italy (1994), p. 493.
37. J. S. Lim, J.-Y. Park, B.-G. Lee, Y.-W. Lee, and J.-D. Kim, *J. Chem. Eng. Data* **44**:1226 (1999).
38. J. S. Lim, J.-Y. Park, B.-G. Lee, and J.-D. Kim, *J. Chem. Eng. Data* **45**:734 (2000).
39. B.-G. Lee, J.-Y. Park, J. S. Lim, and Y.-W. Lee, *J. Chem. Eng. Data* **45**:760 (2000).
40. P. Sliwinski, *Z. Phys. Chem. Neue Folge* **63**:263 (1969).
41. R. W. Benoliel, Thesis (Pennsylvania State College, State College, 1941).
42. J. B. Rodosevich and R. C. Miller, *AIChE J.* **19**:729 (1973).
43. C. R. McClune, *Cryogenics* **16**:289 (1976).
44. W. M. Haynes and M. J. Hiza, *J. Chem. Thermodyn.* **9**:179 (1977).
45. J. E. Orrit and J. M. Laupretre, *Adv. Cryog. Eng.* **23**:573 (1978).
46. R. Masui, W. M. Haynes, R. F. Chang, H. A. Davis, and J. M. H. Levelt Sengers, *Rev. Sci. Instrum.* **55**:1132 (1984).
47. G. Kaminishi, C. Yokoyama, and S. Takahashi, *Sekiyu Gakkaishi* **31**:433 (1988).
48. G. S. Parks, C. H. Shomate, W . D. Kennedy, and B. L. Crawford, Jr., *J. Chem. Phys.* **5**:359 (1937).
49. R. D. Goodwin and W. M. Haynes, *NBS Technical Note 1051* (U.S. Deptartment of Commerce, Washington, DC, 1982), p. 196.
50. NGAA, *Oil Gas J.* **44**:115 (1945).
51. R. Matteson, *ASTM Special Tech. Publication* No. 109 (1950).
52. T. R. Das, C. O. Reed, and P. T. Eubank, *J. Chem. Eng. Data* **18**:253 (1973).
53. J. M. H. Levelt Sengers, B. Kamgar-Parsi, and J. V. Sengers, *J. Chem. Eng. Data* **28**:354 (1983).
54. K. Stephan and H. Hildwein, *Recommended Data of Selected Compounds and Binary Mixtures (Chemistry Data Series) Dechema 4* (1987).
55. H.-L. Zhang, Sharp Corp., Shinjo, Nara, Japan, private communication (1999).
56. P. J. Mohr and B. N. Taylor, *J. Phys. Chem. Ref. Data* **28**:1713 (1999).
57. T. B. Coplen, *J. Phys. Chem. Ref. Data* **26**:1239 (1997).
58. S. S. Chen, R. C. Wilhoit, and B. J. Zwolinski, *J. Phys. Chem. Ref. Data* **4**:859 (1975).
59. M. Jaeschke and P. Schley, *Int. J. Thermophys.* **16**:1381 (1995).
60. R. Span, *Multiparameter Equations of State—An Accurate Source of Thermodynamic Property Data* (Springer, Berlin, 1999).
61. H.-L. Zhang, S. Tada, and K. Watanabe, *Proc. 19th Jpn. Symp. Thermophys. Prop.*, Fukuoka, Japan (1998) [in Japanese], p. 311.
62. T. O. Lüddecke and J. W. Magee, *Int. J. Thermophys.* **17**:823 (1996).
63. L. A. Weber, *Int. J. Refrig.* **17**:117 (1992).